Impurity density gradient influence on trapped particle modes

M. Idouakass, E. Gravier, M. Lesur, J. Médina, T. Réveillé, T. Drouot, X. Garbet, and Y. Sarazin

Impurity density gradient influence on trapped particle modes

M. Idouakass,[1] E. Gravier,[1] M. Lesur,[1] J. Médina,[1] T. Réveillé,[1] T. Drouot,[1] X. Garbet,[2] and Y. Sarazin[2]

[1]*Institut Jean Lamour, UMR 7198 CNRS, Université de Lorraine, 54000 Nancy, France*
[2]*CEA-IRFM, 13115 Saint-Paul-Lèz-Durance, France*

The effect of the presence of an impurity species on the trapped particle turbulence is studied using the gyro-bounce kinetic code TERESA, which allows the study of Trapped Electron Modes and Trapped Ion Modes. The impurity species is treated self-consistently and its influence on the nature of the turbulence, ion driven or electron driven, is investigated. It is found that the presence of heavy impurities with a flat density profile tends to stabilize the both electron and ion modes, whereas a peaked or hollow impurity density profile can change the turbulence from an electron driven turbulence to an ion driven turbulence. The effect of the turbulence regime on impurity transport is studied. https://doi.org/10.1063/1.5026381

I. INTRODUCTION

In tokamak physics, impurities are defined as particles of the plasma that are not part of the elements that contribute to the reaction of fusion. Impurity transport is an issue that needs to be understood in order to obtain a sustainable burning plasma. These impurities can have different sources; they can come from the plasma boundaries, where particles are sputtered from the walls: in this case the impurity species will be tungsten in the context of ITER or can be carbon in other machines (such as JT60-SA). In addition, other species, such as argon or neon, can be introduced into the plasma edge in order to decrease the heat and particle fluxes on the walls and these particles can then propagate into the plasma core. On the other hand, the impurities can come from the plasma core, in which case they are α-particles produced by the reactions of fusion.

These impurities can have negative effects on the plasma confinement in two major ways. First, they may contribute to plasma dilution, reducing the fuel present for a given pressure. Second, these impurities are ionized multiple times, and through cycles of ionization-recombination and excitation-deexcitation, will radiate a significant part of the plasma energy from the core.

It is therefore very important to understand impurity transport so that accumulation in the plasma core can be avoided. The direction of this transport, i.e., inwards or outwards, does not solely depend on the impurity density gradient. Indeed, neoclassical theory predicts a pinch velocity depending on both the main ion density gradient and temperature gradient. In addition, turbulence also contributes to impurity flux, with a sign that depends on the type of dominant instability, whether it is electron or ion driven.

Flat, peak, and hollow profiles of impurities can be realized in experiments. For instance in Alcator C-mod[1,2] hollow or flat profiles can be observed during a H-mode, peaked for instance at mid-radius and hollow near the core. In ASDEX, it has been shown that Ion Cyclotron Resonance Heating (ICRH) power coupling could be optimized to reduce the tungsten influxes, and the use of Electron Cyclotron Resonance Heating (ECRH) allows keeping the central peaking of the tungsten concentration low.[3,4] In JET with its

ITER-like wall (JET-ILW) operation, it is observed that $n > 1$ tearing modes can significantly speed the on-axis peaking of tungsten impurities, which in-turn degrades core confinement through radiative losses.[5] Also high-Z impurity transport from the plasma edge to the core appears to be a dominant factor to explain the observations.[6,7] Some models have been introduced to describe the high-Z concentration in the plasma core.[8] The critical behavior of the central tungsten concentration in some experimental scenarios could be attributed to edge and core transport parameters. For example, one of the most critical scenarios appears to be a hot edge combined with peaked density profiles.

Significant progress has been made in the investigation of turbulent transport of impurity ions in recent years. Fluid models[2,9] or gyrokinetic codes such as GYRO, GENE, and GKW containing realistic tokamak geometry,[10] auxiliary heating,[11] collisionality,[12] rotational shear,[13] toroidal rotation,[14] and poloidal asymmetries[15] have been successfully employed in the studies. Also the impact of the neoclassical distribution function on turbulent impurity and momentum fluxes has been recently investigated using fluid and gyrokinetic simulations.[16]

In this work, we focus on turbulence issues. More precisely, we look at the influence of the impurity profile on trapped particle driven modes and study the transport of these impurities. This is done using the code TERESA, which is a semi-Lagrangian code based on a collisionless reduced bounce-averaged gyrokinetic model.[17–22] This code treats the passing particles adiabatically and allows the study of Trapped Electron Modes (TEM) and Trapped Ion Modes (TIM). Its most interesting property is that it enables the full-f treatment of multiple populations of trapped particles at low numerical cost. However, the model on which the TERESA is based is collisionless, and as such it can only provide the turbulent contribution to transport.

In the high temperature and low collisionality regime relevant for ITER, collisionless turbulent transport contribution is expected to dominate over the neoclassical contribution for light impurities.[23]

For heavy impurities, while the contribution of neoclassical (collisional) transport and the interplay between

turbulent and neoclassical transport need to be taken into account to have a complete understanding of impurity transport, obtaining a clear picture of the purely turbulent impurity transport is a necessary step towards this final objective.

TERESA allows the processing of trapped ions, electrons, and impurities. This enables us to observe the action of the impurities as an active species, i.e., taken into account in the quasineutrality constraint, thus seeing how they influence the dynamics of the plasma, particularly on the instability growth rates and on the nonlinear phase.

Of course in this TERESA model kinetic physics of passing particles is missing. Nevertheless, as heavy impurities have a much smaller parallel velocity (factor $\sqrt{A}$ with A the mass number) they will therefore have a parallel velocity too small to resonate with the TIM or TEM carried by the main trapped ions and trapped electrons.

We will show that by changing the radial gradient of impurities in an otherwise identical plasma, it is possible to move from a TEM dominated turbulence to a TIM dominated turbulence. In addition, we show depending on the dominant regime of turbulence, the importance of the zonal flow and thus of transport changes.

In Sec. II, the model used in this paper is briefly described, and then it is used to perform the linear analysis in Sec. III where it is shown how impurities modify the linear growth rate of the instability. In Sec. IV, numerical results on zonal flow generation and transport are discussed. Finally, a brief summary of the results along with a conclusion is given.

II. MODEL—TERESA CODE

The TERESA code is based on an electrostatic reduced bounce averaged gyrokinetic model.[17,22,24,25] The dynamics that will be considered here evolves on timescales of the order of the trapped particles precession frequency. Therefore, it is possible to gyro-average and bounce-average the Vlasov equation, thus filtering out the fast frequencies ω_C (cyclotron frequency) and ω_b (bounce frequency) and the small space scales ρ_c (gyro-radius) and δ_b (banana width). The trapped particles are treated kinetically, while the passing particles are treated adiabatically.

This allows one to reduce the dimensionality from 6D to 4D. It is furthermore possible to adopt an action-angle formalism, simplifying the treatment of the Vlasov equations. Finally, only two variables appear in the differential operators: the angle $\alpha = \varphi - q\theta$ and the magnetic flux ψ where φ is the toroidal angle, θ is the poloidal angle, and q is the safety factor. The variable ψ is a function of the minor radius and will be used as a radial coordinate for the numerical simulations. The other two dimensions are two invariants: the particle kinetic energy E and the trapping parameter κ.

Using these reductions, the Vlasov equation reads

$$\frac{\partial f_s}{\partial t} - [J_{0,s}\phi, f_s]_{\alpha,\psi} + \frac{\Omega_d E}{Z_s}\frac{\partial f_s}{\partial \alpha} = 0. \tag{1}$$

Here, f_s is the gyro-bounce-averaged particle distribution function, with the subscript $s = i, e, z$ indicating the species considered (main ion, electron, or impurity), and ϕ is the

plasma potential. The Poisson brackets are defined as $[g, h] = \partial_\alpha g \partial_\psi h - \partial_\alpha h \partial_\psi g$. Z_s is the charge number.

$\Omega_d = \frac{Z_s \omega_{d,s}}{E}$, with $\omega_{d,s}$ the toroidal precession frequency for the species s that can be expressed[26] as follows:

$$\omega_{d,s} = \frac{q}{a}\frac{E}{q_s B_{min} R_0}\bar{\omega}_d, \tag{2}$$

where q is the safety factor, a is the minor radius of the tokamak, q_s is the electric charge of the species s, B_{min} is the minimal strength of the magnetic field on a field line, E is the kinetic energy, and $\bar{\omega}_d$ is defined as follows:[26]

$$\bar{\omega}_d = \frac{2\mathcal{E}(\kappa^2)}{\mathcal{K}(\kappa^2)} - 1 + 4s_0\left(\frac{\mathcal{E}(\kappa^2)}{\mathcal{K}(\kappa^2)} + \kappa^2 - 1\right), \tag{3}$$

where $\kappa = \sqrt{\frac{1-\lambda}{2\varepsilon\lambda}}$ is the trapping parameter, $\varepsilon = \frac{a}{R_0}$ is the inverse of the aspect ratio of the tokamak, $\lambda = \mu B_{min}/E$, s_0 is the magnetic shear, and $\mathcal{K}(\kappa^2)$ and $\mathcal{E}(\kappa^2)$ are, respectively, the complete elliptic functions of the first and second kinds. Clearly, the precession frequency does not depend on the mass of the particle and the charge alone appears in this expression. In conclusion, the electron toroidal precession and the main ion ($Z_s = 1$) toroidal precession present the same space-time scales, which enables the construction of a kinetic model including both TIM and TEM regimes with a minimum of numerical constraints.

In this paper, we will consider a single value $\kappa = 0$, corresponding to deeply trapped particles. This further reduces the dimensionality from 4D to 3D. Moreover, we assume that the magnetic shear is constant over radius.

The gyro-bounce-averaging operator is approximated as

$$J_{0,s} = \left(1 - \frac{E}{T_{eq,s}}\frac{\delta_{b0,s}^2}{4}\partial_\psi^2\right)^{-1}\left(1 - \frac{E}{T_{eq,s}}\frac{q^2\rho_{c0,s}^2}{4a^2}\partial_\alpha^2\right)^{-1}, \tag{4}$$

where $\rho_{c0,s}$ and $\delta_{b0,s}$ are the Larmor radius and the banana width (expressed in units of ψ) at an arbitrary typical temperature T_0 (energy is normalized to the typical thermal energy T_0), $\delta_{b0,s} = q\rho_{c0,s}/\sqrt{\varepsilon}$ and $T_{eq,s}$ is the equilibrium temperature at $\psi = 0$. $\omega_0 = T_0/(eR_0^2 B_\theta)$ corresponds to the ion precession frequency at the typical temperature T_0 (time is normalized to this frequency which in tokamaks is of the order of 10^3 rad s^{-1}) and $L_\psi = aR_0 B_\theta$ is the radial length of the simulation box in units of ψ. L_ψ and ω_0 are arbitrarily chosen equal to 1.

The quasi-neutrality equation reads

$$\frac{2}{\sqrt{\pi}}\frac{T_{eq,i}}{T_0}\sum_s\left(Z_s\mathscr{C}_s\int_0^\infty J_{0,s}f_s E^{1/2}dE\right)$$
$$= C_{ad}\left(\phi - \varepsilon_\phi\langle\phi\rangle_\alpha\right) - C_{pol}\sum_s\mathscr{C}_s\tau_s Z_s^2\Delta_s\phi, \tag{5}$$

where $\mathscr{C}_s = n_s/n_{eq}$ is the concentration (n_s is the population density, $n_{eq} = n_{0,e}$ is the equilibrium density, and we have $\sum_s Z_s n_s = 0$), $C_{pol} = e\omega_0 L_\psi/T_0$, $C_{ad} = C_{pol}\frac{1-f_T}{f_T}\sum_s(Z_s^2\mathscr{C}_s\tau_s)$ where f_T is the fraction of trapped particles and $\tau_s = T_{eq,i}/T_s$. The operator Δ_s is defined as $\Delta_s = (\frac{q\rho_{c0,s}}{a})^2\partial_\alpha^2 + \delta_{b,0}^2\partial_\psi^2$ and

$\varepsilon_\phi = (\sum_s \tau_s \mathscr{C}_s Z_s^2 \varepsilon_{\phi,s})/(\sum_s \tau_s \mathscr{C}_s Z_s^2)$. ε_ϕ is a control parameter which governs the response of the adiabatic passing particles. Regarding the electron response, $\varepsilon_{\phi,e} = 1$ prevents the passing electrons from responding to the zonal potential which is constant on a flux surface (toroidal mode $n = 0$). This situation prevails when the electron gyro-radius is small compared with the characteristic length of the zonal flows.[27] Unlike passing electrons, passing ions must respond to zonal flows ($0 \leq \varepsilon_{\phi,i} \leq 1$); therefore, ε_ϕ should be in the range [0, 1]. The model does not allow the adiabatic response to be properly computed so we introduce ε_ϕ as a free parameter and assume the form chosen in Eq. (5). A detailed study of this parameter was performed in Ref. 28. Hereafter, only the extreme case $\varepsilon_\phi = 1$ is considered.

III. LINEAR THEORY

A. Dispersion relation

Linearizing Eqs. (1) and (5) yields a linear dispersion relation which can be solved to find the growth rate and real frequency of the TEM and TIM for different plasma parameters. The dispersion relation reads

$$D = 0 = C_n - \sum_s C_s \tau_s \int_0^\infty J_{n,s}^2$$
$$\times \frac{\kappa_{n,s} + \kappa_{T,s}\left(\xi_s - \frac{3}{2}\right)}{\Omega_d(\xi_s - W_s)} e^{-\xi_s} \xi_s^{\frac{1}{2}} d\xi, \tag{6}$$

where the equilibrium distribution function has been approximated by

$$F_{eq,s} = \frac{n_{0,s}}{T_{eq,s}^{\frac{3}{2}}} e^{-\xi_s}\left[1 + \psi\left(\kappa_{n,s} + \kappa_{T,s}\left(\xi_s - \frac{3}{2}\right)\right)\right] \tag{7}$$

and the coefficient C_n is defined as $C_n = \frac{\sqrt{\pi}}{2}[C_{ad} + C_{pol}n^2 \sum_s \mathscr{C}_s \tau_s Z_s^2 \rho_{C,s}^2 + C_{pol}k^2 \sum_s \mathscr{C}_s \tau_s Z_s^2 \delta_{b,s}^2]$. Here, $\xi = \frac{E}{T_{eq,s}}$, $W_s = \frac{Z_s \omega}{n \Omega_d T_s}$, n being the mode number in the α-direction, $k = \pi$ the most unstable radial mode, and ω the mode frequency. The inverse radial gradient lengths are given by $\kappa_{n,T} = \partial_\psi \log(n_{eq}, T_{eq})$.

B. Presence of an impurity species

Using this dispersion relation, we investigate the effect of introducing an impurity species. Here and in the remainder of the paper, we consider a plasma composed of deuterium as the single main ion species and tungsten W^{40+} ($Z = 40$) as a single impurity species.

1. Impurities with no radial density gradient

Let us first look at a situation where there is no radial density gradient. The parameters are given in Table I. It should be noted that the Larmor radii and banana widths are constant and do not vary with ψ. Densities and temperatures ($n_{0,s}$ and $T_{0,s}$) are given at the edge of the radial box and profiles vary with ψ according to these values at the edge and ($\kappa_{n,s}, \kappa_{T,s}$).

Simulations are not performed with actual ion to electron mass ratio ($m_i/m_e = 9$, see Table I), but they are performed with actual impurity mass to main ion species ratios ($m_Z/m_i = 184/2$, corresponding to $\rho_{c_Z} = 0.24\rho_{c_i}$ with $Z = 40$). We have chosen these parameters so that we deal with modes in the range $n = 8$ to $n = 20$. Our purpose is to get a trend. Actually, if we try to deal with actual ion and electron parameters, then we need to consider a more accurate grid in the α direction.

Figure 1 shows the growth rate of TIMs and TEMs as a function of the tungsten concentration $\mathscr{C}_z$. In the ratio $\mathscr{C}_z$, only n_Z is changed. n_0 is the electron density and remains constant (equal to 1). The densities have to satisfy the quasi-neutrality constraint: as a consequence, the main ion density decreases as $\mathscr{C}_z$ increases.

Consistently with Refs. 29–32, we observe that the impurities, for flat density profiles, have a stabilizing effect on trapped particle modes due to increased dilution, and that this stabilizing effect increases with the impurity concentration. We also observed that real frequencies decrease with the tungsten impurity concentration.

It is worth noticing that by increasing impurity concentration, the coefficient C_{ad} increases according to the definition of C_{ad}. This factor plays a major role in determining the instability growth rates, regardless of the nature of the instability. A large C_{ad} means a large adiabatic response of the passing particles leading to a decrease in the instability growth rate.

It should be noted that we also observed that the TIMs and TEMs are stabilized more easily by impurity species with a higher charge number. This also shows that, in the cases we are studying, the impurities cannot be treated as
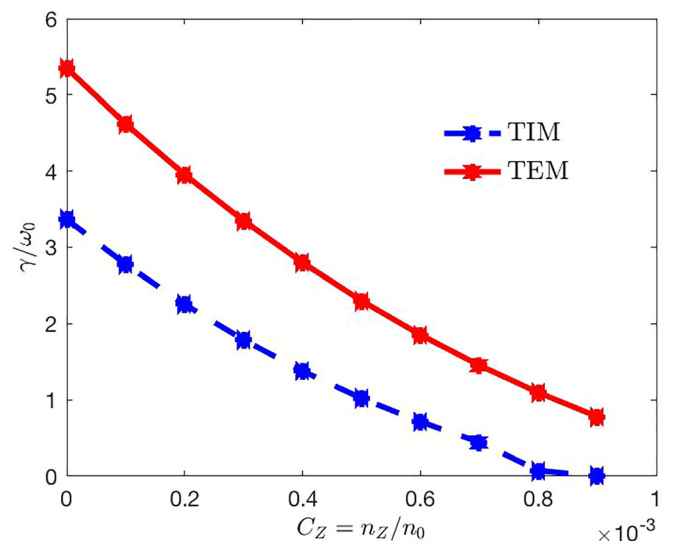

FIG. 1. Growth rate of the fastest growing mode of TIMs and TEMs as a function of the tungsten impurity density $\mathscr{C}_z$. Only n_Z is changed, n_0 is the electron density and remains constant. The blue dots correspond to TIM growth rates and the red dots correspond to TEM growth rates.

TABLE I. Typical plasma parameters used.

n_{e_0}	$\frac{m_e}{m_i}$	$\frac{m_Z}{m_i}$	ρ_{c_e}	ρ_{c_i}	ρ_{c_Z}	δ_{b_e}	δ_{b_i}	δ_{b_Z}	$\kappa_{T,s}$	$\kappa_{n,s}$	τ_e	τ_Z
1	0.11	92.0	0.01	0.03	0.0072	0.01	0.1	0.024	0.25	0	1	1

TABLE II. Parameters for cases with an impurity density gradient.

κ_{n_i}	κ_{T_Z}	$\mathscr{C}_i$	$\mathscr{C}_z$	$\mathscr{C}_e$
0.05	0.25	0.968	0.0008	1

traces, and their action on the plasma needs to be taken into account.[33]

Finally it is worth noticing that if we want to increase the ion to electron mass ratio, as a consequence the most linearly unstable mode increases. Nevertheless, the linear results remain in qualitative agreement with the results presented here: The linear growth rates decrease with the impurity density.

2. Influence of the radial density gradient

We will now look at the influence of a radial density gradient of impurities. For this study, the impurity profile is varied and the quasi-neutrality constraint is ensured

$$n_e = n_i + Zn_Z. \tag{8}$$

Let us first define the relative impurity gradient length as $G_Z = \kappa_{n_Z}/\kappa_{n_i}$. The parameters of the simulations shown in this section are displayed in Table II. The parameters not shown are the same as those in Table I. It should be noted that κ_{n_i} will remain constant in the rest of the paper and be equal to 0.05, except when comparisons with the case κ_{n_e} constant will be needed.

We show two cases in Fig. 2, corresponding to a population of tungsten impurities with the same concentration, but opposite gradients $G_Z = \pm 20$. Note that this value is large mainly because $\kappa_{n,i}$ is small. In this situation, the linear analysis shows that for an impurity profile peaked ($G_Z > 0$) the TEMs are the most linearly unstable [see Fig. 2(a)]. On the other hand, when the impurity profile is hollow ($G_Z < 0$), the TIMs are the most linearly unstable but dominant only in the low mode range, while TEMs are dominant beyond $n = 10$ and stay unstable even when TIMs are stable [see Fig. 2(b)].

We observe that the gradient of heavy impurities, when it is in the same direction as the main ion species gradient,

will decrease the TIM growth rate and increase the TEM growth rate, whereas it will increase the TIM growth rate and decrease the TEM growth rate when these gradients are in opposing directions.

It should be noted that the same simulations but with the electron density gradient held fixed (and the ion density gradient allowed to change) would give results that are qualitatively close to those presented in Fig. 2.

We provide a basic explanation for this linear behaviour. Using the quasi-neutrality constraint and the definitions used before, we can write:

$$\kappa_{n_e} = \mathscr{C}_i \kappa_{n_i} + Z \mathscr{C}_Z \kappa_{n_Z}. \tag{9}$$

With the parameters given in Table II, we obtain a large value of the electron density gradient $\kappa_{n_e} = 0.0804$ in the case $G_Z = +20$ [Fig. 2(a)], which destabilizes TEM instabilities. On the other hand, with $G_Z = -20$ [Fig. 2(b)], the electron density gradient is smaller and $\kappa_{n_e} = 0.0164$. This result is consistent with the fact that the collisionless trapped electron modes, driven unstable by resonance with the trapped toroidal precession drift, are shown[26,34] to be unstable with a growth rate that increases with κ_{n_e}.

This result is also consistent with results from nonbounce-averaged gyrokinetic simulations discussed in Refs. 29 and 32, where it was shown that the TEM growth rate increases with the impurity density gradient in the case of a relatively flat density profile. This trend is also observed in Fig. 3, which displays the linear growth rate of the fastest growing TIM and TEM for different impurity density gradients. In addition, we can see in Fig. 3 a transition between TIM dominated dynamics and TEM dominated dynamics occurring around $G_Z = -18$ (solid curves, $\kappa_{n,i} = 0.05$) for the parameters considered here. It should be noted that, by keeping a fixed electron gradient $\kappa_{n,e} = 0.05$ and adapting the ion profile to ensure electroneutrality, the results displayed in Fig. 3 remain qualitatively similar (dotted curves), with the difference that the transition from TIM to TEM occurs around $G_Z = -12$.

The behavior of real frequencies ω_r also remains similar: The TEM real frequency increases with G_Z, whereas the TIM real frequency decreases with G_Z. But the variation is
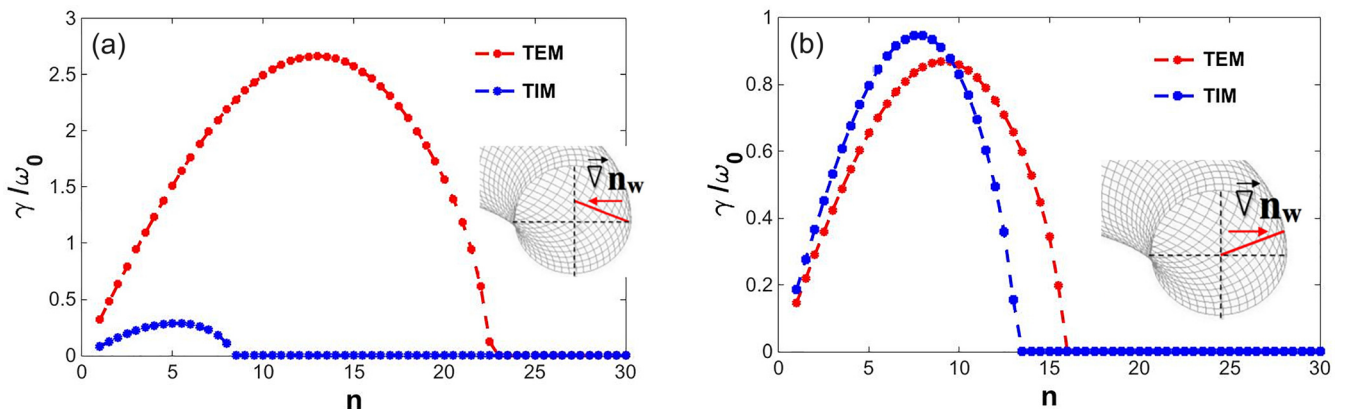

FIG. 2. Growth rate of TEMs and TIMs as a function of mode number. Case (a) $G_Z = +20$, case (b) $G_Z = -20$. The blue dashed curve corresponds to the growth rate of the TIM modes and the red solid curve corresponds to the growth rate of the TEM modes. For clarity, negative growth rates have been set to zero. The poloidal cross section sketches display the shape of the impurity profile for negative and positive G_Z.
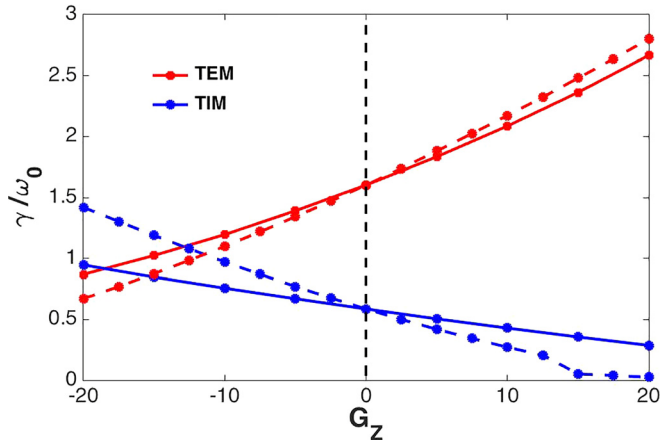
FIG. 3. Linear growth rate of the fastest growing mode as a function of the impurity gradient length G_Z. The blue solid (dotted) curve corresponds to TIM growth rates; the red solid (dotted) curve corresponds to TEM growth rates, keeping κ_{n_i} (κ_{n_e}) constant.

not strong: For instance in the case keeping $\kappa_{n,e}$ constant, for TEM the real frequency changes from $\omega_r = -13$ ($G_Z = -20$) to -16 ($G_Z = +20$) while for TIM the real frequency changes from $\omega_r = 6.7$ ($G_Z = -20$) to 6.58 ($G_Z = +20$).

Finally, according to Eq. (9), since a big G_Z value leads to a big ratio $\kappa_{n,e}/\kappa_{n,i}$, indicating a small ratio ion/electron drift frequency, the Landau damping of main ions is increased, stabilizing the TIM modes, while the free energy is transferred from trapped electrons to waves via wave-precession drift resonance and thus the TEMs become more unstable.

IV. NONLINEAR SIMULATIONS

The numerical simulations are done using a thermal and density bath as boundary conditions, i.e., the temperature and density are fixed at both radial boundaries $\psi = 0$ (outer boundary) and $\psi = 1$ (inner boundary). Dirichlet boundary conditions are imposed on the potential. The grid mesh is $N_\alpha = 257$, $N_\psi = 513$, and $N_E = 192$ for the energy parameter. An initial perturbation is imposed on the electrostatic potential, with all modes excited with a small amplitude and random phases.

First, let us note that there is a good agreement between the linear analysis prediction for the growth rates and the ones obtained from direct, initial value, numerical simulations. In addition, the direction of propagation of the instability (ion precession direction for TIMs and electron precession direction for TEMs) is recovered, depending on the peaked ($G_Z = +20$) or hollow ($G_Z = -20$) impurity density profile. There is a small difference in the numerical and analytical linear growth rates, leading to a transition from TIM dynamics to TEM dynamics for $G_Z \simeq -14$ numerically. This difference is due to the assumptions made in the linear theory.

A. Influence of the dominant mode on the zonal flow

An interesting quantity to consider when investigating the importance of the zonal flow is its energy compared to that of the other modes. This ratio can be calculated as[21]

$$\frac{W_{ZF}}{W_{n \neq 0}} = \frac{\int_0^1 \left\langle \frac{\partial \phi}{\partial \psi} \right\rangle_\alpha^2 d\psi}{\int_0^1 \left\langle \left(\frac{\partial \phi}{\partial \psi} - \left\langle \frac{\partial \phi}{\partial \psi} \right\rangle_\alpha \right)^2 \right\rangle_\alpha d\psi}, \quad (10)$$

where W_{ZF} is the zonal flow energy and $W_{n \neq 0}$ is the energy contained in all other modes.

In Fig. 4, the time evolution of the amplitude of different modes is given, and the zonal flow amplitude is highlighted. The two cases shown here are the ones discussed previously. In the saturated phase, we observe that the ratio $W_{ZF}/W_{n \neq 0}$ is much larger when TIMs dominate the dynamics [Fig. 4(a)] than when TEMs dominate the dynamics [Fig. 4(b)]. In the case $G_Z = -20$ (TIM), the ratio is $W_{ZF}/W_{n \neq 0} \simeq 3500$, while in the case $G_Z = +20$ (TEM), the ratio is $W_{ZF}/W_{n \neq 0} \simeq 80$.

It appears, consistently with Ref. 27, that this behaviour is intrinsic to TEM and TIM turbulence and has nothing to do with the presence of impurities, but whether the dominant mode is an electron or an ion driven mode. Here, this dominant mode depends on the impurity profile. For example, in the case of a hollow impurity profile, with $G_Z = -5$, the
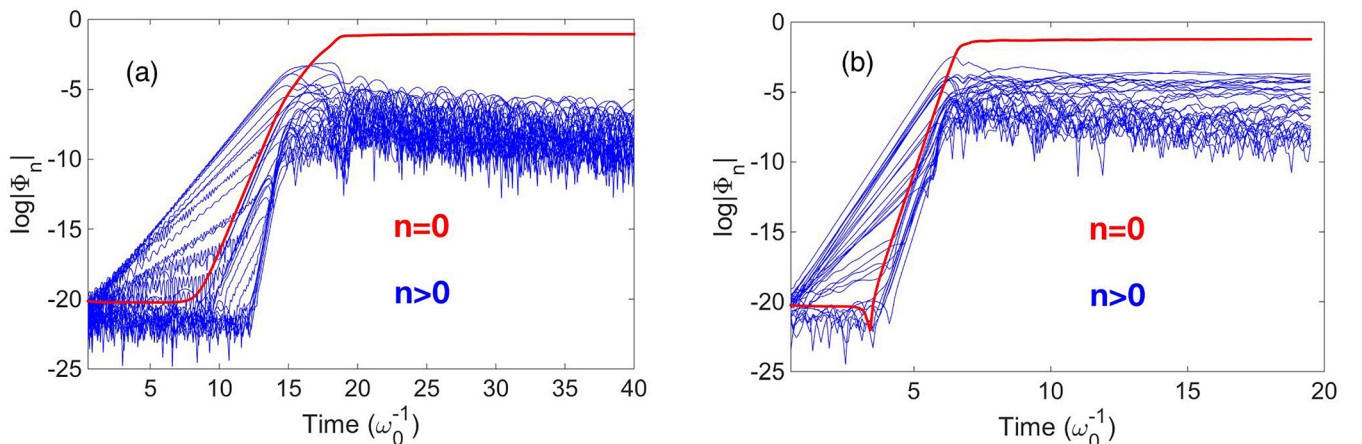

FIG. 4. Temporal evolution of the potential amplitude, for $n = 0$ to $n = 30$. The mode $n = 0$ is highlighted in red. Case (a): $G_Z = -20$ where TIMs are dominant; case (b): $G_Z = +20$ where TEMs are dominant.

dominant mode is a TEM and the ratio is of the order of $W_{ZF}/W_{n\neq0} \simeq 100$.

It should be noted that these ratios are high in all cases due to the parameters chosen, so the ratios are relevant considered with respect to one another.

In the TIM turbulence, the trapped electron gyroradius and banana width, when compared to the characteristic length of turbulence, are smaller than in the case of TEM turbulence, because the characteristic length is smaller in the TEM case. Therefore, in the TIM regime trapped electrons cannot respond across the zonal flow potential that is constant on a flux surface, and as a result, zonal flows can be strong. In the TEM regime, trapped electrons can respond more and consequently zonal flows become less strong.

As mentioned before, regarding passing particles, it should also be noted that taking $\varepsilon_\phi = 1$ means to suppress any response from passing particles to zonal flow potential. For linear studies, the value of ε_ϕ does not change the nature of the instability and the linear growth rate of the instability remains the same. For the results displayed in Fig. 4, by considering $\varepsilon_\phi = 0.5$ for instance a change of the saturation level of zonal flows is observed, but the ratio between the energy contained in zonal flows in the TEM case and in the TIM case remains substantially the same. In this paper, we only show a trend and we chose to consider the case $\varepsilon_\phi = 1$.

B. Impurity transport

In this section, we will investigate the transport of particles when impurities are present. The particle flux is defined as[22]

$$\Gamma_s = -\frac{2}{\sqrt{\pi}} \int d\alpha \int \frac{\partial J_{0,s}\phi}{\partial\alpha} f_s E^{\frac{1}{2}} dE. \qquad (11)$$

The impurity particle flux can be modeled as the sum of a diffusive flux and a convective flux

$$\Gamma_Z = -D\nabla n_Z + V n_Z, \qquad (12)$$

where D is a diffusion coefficient and V is a pinch velocity.

This Eq. (12) can also be written in the form

$$\frac{\Gamma_Z}{n_e \mathscr{C}_Z} = -D G_Z \kappa_{n_i} + V. \qquad (13)$$

We first note that when there is a peaked impurity profile ($G_Z > 0$), the TEMs dominate the dynamics and the transport is dominated by the electrons. In this case, the impurity particle and heat fluxes are outward.

On the other hand, when the impurity profile is hollow, either the TIMs or the TEMs can dominate the dynamics, but in both cases, the impurity particle flux is inward.

Figure 5 shows the impurity particle flux Γ_z, averaged over the spatial variables, and averaged over time, as a function of G_Z. We see that there are different transport regimes depending on the radial impurity density gradient.

Let us first look at the range $-20 < G_Z < -15$. This is a range of parameters where the TIMs dominate the dynamics, and we can see that there is a weak dependence of the transport on the impurity density gradient.
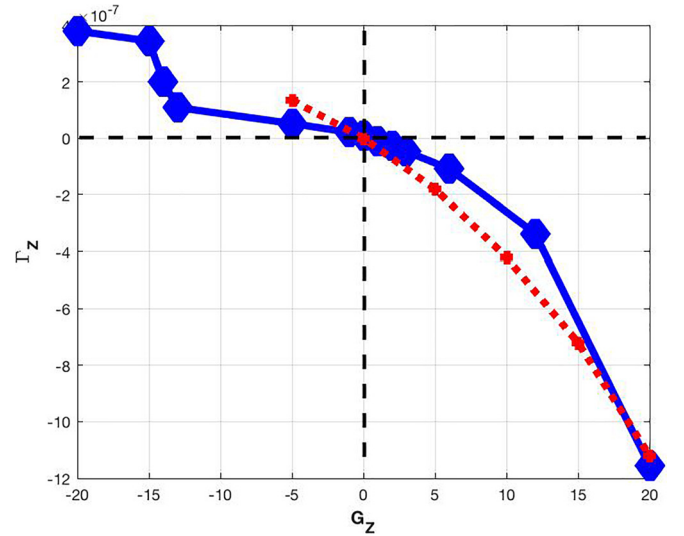

FIG. 5. Averaged impurity flux Γ_z as a function of G_Z. The dots correspond to simulation points (in blue). In red (dotted line) is shown the particle flux estimated from the mixing length estimate ($\Gamma_z \propto -\gamma G_Z$) and using the linear growth rates of the TEM instability as a function of G_Z (see Fig. 3).

In the next range, $-15 < G_Z < -12$, there is a competition between TIMs and TEMs, and we can observe a strong decrease in the transport with a small increase in the gradient. This is likely due to a transition from the ion driven to the electron driven turbulent regime.

This leads to a range $-12 < G_Z < +6$ where the particle flux scales close to linearly, but there is a change of transport coefficient depending on the sign of G_Z, with a transport coefficient in the peaked profile larger than in the hollow profile. However, the transition from inward to outward transport occurs very close to $G_Z = 0$, which indicates that in that turbulent regime, the pinch effect is negligible compared to the turbulent transport. Indeed, in a zero-flux situation, the pinch velocity can be obtained as $V = (D\nabla n_Z)/n_Z$, which is zero for a flat density profile. It should be noted that the current implementation of the TERESA code does not allow the description of either the curvature pinch or the neoclassical pinch associated with the collision operator, which may explain the fact that no pinch is observed.

Then in the range $+6 < G_Z < +20$, the transport increases with a rate faster than linear with respect to G_Z. To provide a basic explanation of this change of slope, we also estimate the flux $\frac{\Gamma_Z}{n_e \mathscr{C}_Z}$ given by (13). We assume that the pinch velocity is zero and that n_e and κ_{n_i} are constant. The flux is thus proportional to $-D G_Z$. Using the mixing length estimate, we assume that the diffusion coefficient is equal to γ/k_r^2, with k_r constant and γ being linear growth rates of the TEM instability as a function of G_Z (see Fig. 3). This estimated flux is also plotted against G_Z in Fig. 5 (in red, dotted line). We observe a qualitative agreement between the flux obtained from nonlinear TERESA simulations and that of given by the mixing length estimate.

It must be noticed that we also performed simulations considering the trapping parameter κ equal to 0.85 instead of 0, i.e., considering barely trapped particles instead of deeply trapped particles. Changing κ leads to modifying $\bar{\omega}_d$ from 1 to 0.16 according to the complete elliptic functions of the

first and second kinds, with a magnetic shear equal to zero [Eq. (3)]. In this case, the plasma behavior is strongly modified. The linear growth rate of the instability is much greater and therefore, the saturation levels of drift waves and zonal flows are different when compared to the previous case considering deeply trapped particles. Moreover, the impurity flux is multiplied by one order of magnitude when compared to that of the $\kappa = 0$ case.

V. CONCLUSION

In this paper, we have studied the impact of the presence of a population of impurities in a tokamak plasma using the gyrokinetic code TERESA. We have shown that their presence can have a strong influence on the dynamics of the turbulence in the plasma. In particular, it was shown that the direction of the radial gradient of impurities could change the nature of turbulence, going from an electron dominated turbulence when the impurity density profile is peaked on the magnetic axis to a trapped ion mode turbulence when the impurity density profile is hollow. It was also shown that the nature of the turbulence could have a strong influence on the relative importance of the zonal flow energy compared to the energy contained in the turbulence, where for ion mode dominated turbulence, the ratio of zonal flow energy to turbulent energy is much greater than that in electron mode dominated turbulence. Finally, we saw that in the case considered here, there was no impurity pinch for a zero-flux situation. Moreover, it appears that the transport of impurities in the case of TEM turbulence and for this set of parameters used in this article is in agreement with the mixing length estimate. In light of these results, it is clear that it is very important when looking at the dynamics of impurities to treat them self-consistently, as their effect on the turbulence can strongly affect their transport.

[1]W. L. Rowan, I. O. Bespamyatnov, and C. L. Fiore, "Light impurity transport at an internal transport barrier in alcator c-mod," Nucl. Fusion **48**(10), 105005 (2008).

[2]S. Futatani, W. Horton, S. Benkadda, I. O. Bespamyatnov, and W. L. Rowan, "Fluid models of impurity transport via drift wave turbulence," Phys. Plasmas **17**, 072512 (2010).

[3]R. Neu *et al.*, Plasma Phys. Controlled Fusion **49**, B59–B70 (2007).

[4]C. Angioni *et al.*, Nucl. Fusion **54**, 083028 (2014).

[5]T. C. Hender, P. Buratti, F. J. Casson, B. Alper, Yu. F. Baranov, M. Baruzzo, C. D. Challis, F. Koechl, K. D. Lawson, C. Marchetto, M. F. F. Nave, T. Pütterich, S. Reyes Cortes, and JET Contributors, "The role of MHD in causing impurity peaking in jet hybrid plasmas," Nucl. Fusion **56**(6), 066002 (2016).

[6]E. Joffrin *et al.*, Nucl. Fusion **54**, 013011 (2014).

[7]R. Neu *et al.*, Phys. Plasmas **20**, 056111 (2013).

[8]A. Kallenbach, R. Neu, R. Dux, H.-U. Fahrbach, J. C. Fuchs, L. Giannone, O. Gruber, A. Herrmann, P. T. Lang, B. Lipschultz, C. F. Maggi, J. Neuhauser, V. Philipps, T. Pütterich, V. Rohde, J. Roth, G. Sergienko, A. Sips, and ASDEX Upgrade Team, "Tokamak operation with high-z plasma facing components," Plasma Phys. Controlled Fusion **47**(12B), B207 (2005).

[9]T. Fulop and H. Nordman, Phys. Plasmas **16**, 032306 (2009).

[10]A. Skyman, L. Fazendeiro, D. Tegnered, H. Nordman, J. Anderson, and P. Strand, Nucl. Fusion **54**, 013009 (2014).

[11]C. Angioni and A. G. Peeters, "Direction of impurity pinch and auxiliary heating in tokamak plasmas," Phys. Rev. Lett. **96**, 095003 (2006).

[12]C. Estrada-Mila, J. Candy, and R. E. Waltz, Phys. Plasmas **12**, 022305 (2005).

[13]Y. Camenen, A. G. Peeters, C. Angioni, F. J. Casson, W. A. Hornsby, A. P. Snodin, and D. Strintzi, Phys. Plasmas **16**, 012503 (2009).

[14]C. Angioni, R. M. McDermott, E. Fable, R. Fischer, T. Putterich, F. Ryter, and G. Tardini, and ASDEX Upgrade Team, Nucl. Fusion **51**, 023006 (2011).

[15]F. J. Casson *et al.*, Plasma Phys. Controlled Fusion **57**, 014031 (2015).

[16]P. Manas, W. A. Hornsby, C. Angioni, Y. Camenen, and A. G. Peeters, Plasma Phys. Controlled Fusion **59**, 035002 (2017).

[17]T. Drouot, E. Gravier, T. Reveille, A. Ghizzo, P. Bertrand, X. Garbet, Y. Sarazin, and T. Cartier-Michaud, "A gyro-kinetic model for trapped electron and ion modes," Eur. Phys. J. D **68**(10), 280 (2014).

[18]T. Drouot, E. Gravier, T. Reveille, and M. Collard, "Self-generated zonal flows in the plasma turbulence driven by trapped-ion and trapped-electron instabilities," Phys. Plasmas **22**(10), 102309 (2015).

[19]T. Drouot, E. Gravier, T. Reveille, M. Sarrat, M. Collard, P. Bertrand, T. Cartier-Michaud, P. Ghendrih, Y. Sarazin, and X. Garbet, "Global gyrokinetic simulations of trapped-electron mode and trapped-ion mode microturbulence," Phys. Plasmas **22**(8), 082302 (2015).

[20]E. Gravier, M. Lesur, T. Reveille, and T. Drouot, "Stimulated zonal flow generation in the case of tem and tim microturbulence," Phys. Plasmas **23**(9), 092507 (2016).

[21]E. Gravier, M. Lesur, T. Reveille, T. Drouot, and J. Médina, "Transport hysteresis and zonal flow stimulation in magnetized plasmas," Nucl. Fusion **57**(12), 124001 (2017).

[22]Y. Sarazin, V. Grangirard, E. Fleurence, X. Garbet, P. Ghendrih, P. Bertrand, and G. Depret, "Kinetic features of interchange turbulence," Plasma Phys. Controlled Fusion **47**, 1817 (2005).

[23]C. Angioni, R. Bilato, F. J. Casson, E. Fable, P. Mantica, T. Odstrcil, M. Valisa, ASDEX Upgrade Team, and JET Contributors, "Gyrokinetic study of turbulent convection of heavy impurities in tokamak plasmas at comparable ion and electron heat fluxes," Nucl. Fusion **57**(2), 022009 (2017).

[24]G. Depret, X. Garbet, P. Bertrand, and A. Ghizzo, "Trapped-ion driven turbulence in tokamak plasmas," Plasma Phys. Controlled Fusion **42**(9), 949 (2000).

[25]T. Cartier-Michaud, P. Ghendrih, Y. Sarazin, G. Dif-Pradalier, T. Drouot, D. Estève, X. Garbet, V. Grandgirard, G. Latu, C. Norscini, and C. Passeron, "Staircase temperature profiles and plasma transport self-organisation in a minimum kinetic model of turbulence based on the trapped ion mode instability," J. Phys.: Conf. Ser. **561**(1), 012003 (2014).

[26]B. Kadomtsev and O. P. Pogutse, *Reviews of Plasma Physics* (Consultants Bureau, New York, 1970), Vol. **5**, p. 249.

[27]X. Garbet, Y. Idomura, L. Villard, and T. H. Watanabe, "Gyrokinetic simulations of turbulent transport," Nucl. Fusion **50**(4), 043002 (2010).

[28]T. Cartier-Michaud, P. Ghendrih, V. Grangirard, and G. Latu, "Optimizing the parallel scheme of the Poisson solver for the reduced kinetic code TERESA," ESAIM:Proc. **43**, 274 (2013).

[29]H. Du, Z.-X. Wang, J. Q. Dong, and S. F. Liu, "Coupling of ion temperature gradient and trapped electron modes in the presence of impurities in tokamak plasmas," Phys. Plasmas **21**(5), 052101 (2014).

[30]R. R. Dominguez and M. N. Rosenbluth, "Local kinetic stability analysis of the ion temperature gradient mode," Nucl. Fusion **29**(5), 844 (1989).

[31]R. Paccagnella, F. Romanelli, and S. Briguglio, "Toroidal ν i mode stability in a multispecies plasma," Nucl. Fusion **30**(3), 545 (1990).

[32]H. Du, Z.-X. Wang, and J. Q. Dong, "Impurity effects on trapped electron mode in tokamak plasmas," Phys. Plasmas **23**(7), 072106 (2016).

[33]N. Bonanomi, P. Mantica, C. Giroud, C. Angioni, P. Manas, S. Menmuir, and JET Contributors, "Light impurity transport in jet ilw l-mode plasmas," Nucl. Fusion **58**(3), 036009 (2018).

[34]J. C. Adam, W. M. Tang, and P. H. Rutherford, Phys. Fluids **19**, 561 (1976).